Apical Vesicles Bearing Inositol 1,4,5-trisphosphate Receptors in the Ca^{2+} Initiation Site of Ductal Epithelium of Submandibular Gland

Miki Yamamoto-Hino,*‡ Atsushi Miyawaki,‡ Akihisa Segawa,§ Eijiro Adachi,§ Shohei Yamashina,§ Toyoshi Fujimoto,‖ Tomoyasu Sugiyama,¶ Teiichi Furuichi,‡ Mamoru Hasegawa,¶ and Katsuhiko Mikoshiba*‡

*Developmental Neurobiology Laboratory, RIKEN Brain Science Institute, Wako-City, Saitama 351, Japan; ‡Department of Molecular Neurobiology, The Institute of Medical Science, University of Tokyo, Minato-ku, Tokyo 108, Japan; §Department of Anatomy and Cell Biology, Faculty of Medicine, Kitasato University, Sagamihara-shi, Kanagawa 228, Japan; ‖Department of Anatomy, School of Medicine, Gunma University, Maebashi-shi, Gunma 371, Japan; and ¶Tokyo Research Laboratories, Kyowa Hakko Kogyo Co., Ltd., Machida-shi, Tokyo 194, Japan

Abstract. In polarized epithelial cells, agonists trigger Ca^{2+} waves and oscillations. These patterns may be caused by the compartmentalization of inositol 1,4,5-trisphosphate (IP_3)-sensitive Ca^{2+} pools into specific regions. We have investigated the relationship between the distribution of IP_3 receptors (IP_3Rs) and the spatiotemporal pattern of Ca^{2+} signaling in the duct cells of the rat submandibular gland (SMG). Using immunofluorescence, although labeling was somewhat heterogeneous, the IP_3Rs were colocalized to the apical pole of the duct cells. Immunoelectron microscopy identified small apical vesicles bearing IP_3R2 in some types of duct cells. Real-time confocal imaging of intact ducts demonstrated that, after carbachol stimulation, an initial Ca^{2+} spike occurred in the apical region. Subsequently, repetitive Ca^{2+} spikes spread from the apical to the middle cytoplasm. These apical Ca^{2+} initiation sites were found only in some "pioneer cells," rather than in all duct cells. We performed both Ca^{2+} imaging and immunofluorescence on the same ducts and detected the strongest immunosignals of IP_3R2 in the Ca^{2+} initiation sites of the pioneer cells. The subcellular localization and expression level of IP_3Rs correlated strongly with the spatiotemporal nature of the intracellular Ca^{2+} signal and distinct Ca^{2+} responses among the rat SMG duct cells.

MANY cellular stimuli, such as hormones, neurotransmitters, and growth factors, evoke an elevation of intracellular Ca^{2+} concentration ($[Ca^{2+}]_i$)[1] (Berridge, 1993). Cytosolic Ca^{2+} signals initiate as Ca^{2+} spikes in a small area near the lumen and then spread as a Ca^{2+} wave toward the basal pole in an oscillatory fashion. This phenomenon occurs in many epithelial cell types, including pancreatic acinar cells (Kasai and Augustine, 1990; Kasai et al., 1993; Thorn et al., 1993, 1996) and hepatocytes (Nathanson et al., 1994). In pancreatic acinar cells, the injection of inositol 1,4,5-trisphosphate (IP_3) causes $[Ca^{2+}]_i$ to increase at the apical zone, suggesting an apical distribution of IP_3-sensitive intracellular Ca^{2+} stores (Kasai et al., 1993; Thorn et al., 1996). IP_3 is an intracellular second messenger signaling molecule that causes release of Ca^{2+} from intracellular stores by binding to an IP_3 receptor (IP_3R), which is a tetrameric Ca^{2+} channel (Maeda et al., 1991). Molecular cloning studies have shown that there are three types of IP_3R derived from distinct genes, termed IP_3R1, IP_3R2, and IP_3R3 (Furuichi et al., 1994). It would be of interest to know where these three types of IP_3R are localized in polarized epithelial cells and if their location is related to the complex pattern of Ca^{2+} signaling in these cells. So far, however, very few immunohistochemical studies on IP_3Rs have covered all three types. Very recently, Lee et al. (1997*a*) characterized the localization of the three types of IP_3R in pancreatic and salivary gland cells in relation to the Ca^{2+} signals and showed that only a small portion of IP_3Rs participate in the initiation of the Ca^{2+} waves.

We investigated localization of IP_3Rs in various rat tissues and found significant amounts of IP_3R2 and IP_3R3 in the apical region of submandibular gland (SMG) duct cells. The amount of IP_3R2 in the duct cells was higher than in any other tissue examined. Moreover, expression

Address all correspondence to Miki Yamamoto-Hino, Department of Molecular Neurobiology, The Institute of Medical Science, The University of Tokyo, Tokyo 108, Japan. Tel.: (81) 3-5449-5319. Fax: (81) 3-5449-5420.

1. *Abbreviations used in this paper*: $[Ca^{2+}]_i$, intracellular calcium concentration; IP_3, inositol 1,4,5-trisphosphate; IP_3R, IP_3 receptor; PSS, physiological salt solution; SMG, submandibular gland.

levels of both IP_3R2 and IP_3R3 in SMG duct varied among the duct cells. This intracellular-polarized and intercellular-heterogeneous distribution of IP_3Rs in SMG duct cells prompted us to perform $[Ca^{2+}]_i$ imaging analysis in relation to the distribution of the IP_3Rs.

In the SMG duct, muscarinic, α- and β-adrenergic agonists were reported to cause mobilization of $[Ca^{2+}]_i$ from the IP_3-sensitive intracellular Ca^{2+} pools (Dehaye and Turner, 1991; Valdez and Turner, 1991; Dehaye et al., 1993; Xu et al., 1996). In the present study, we analyzed the pattern of Ca^{2+} mobilization induced by carbachol (a muscarinic agonist) application using real-time confocal microscopy. We observed oscillatory $[Ca^{2+}]_i$ changes that took place at a frequency of 0.5 Hz. Such rapid $[Ca^{2+}]_i$ changes have not been reported in nonexcitable cells. Ca^{2+} initiation sites producing the $[Ca^{2+}]_i$ change were localized exclusively to the apical poles, where IP_3Rs were concentrated. Moreover, we saw that Ca^{2+} signaling was heterogeneous among the ductal cells: some showed rapid and dynamic Ca^{2+} mobilization, while others responded slowly. The difference was correlated with the heterogeneous expression level of IP_3Rs, which was confirmed by immunofluorescence in the same ducts as those used for Ca^{2+} imaging.

To determine further the ultrastructural localization of IP_3Rs, we performed modified-preembedding, silver-enhanced immunoelectron microscopy. It revealed that the IP_3R2 was predominantly on the small vesicles located in the apical cytoplasm of certain duct cells. This localization appears to be distinct from other known IP_3R sites, such as the ER in Purkinje cells (Mignery et al., 1989) and or calciosomes (Volpe et al., 1988). These results led us to hypothesize the existence of a unique population of "pioneer cells," which possess these apical vesicles and serve as an IP_3-sensitive Ca^{2+} pool to regulate Ca^{2+} signaling throughout the duct.

Materials and Methods

Antibodies

mAbs against IP_3R1, 2, and 3 were designated KM1112 (IgG_1), KM1083 (IgG_{2a}), and KM1082 (IgG_1), respectively. They were raised against synthetic peptides corresponding to the COOH-terminal regions of the human IP_3Rs, the sequences of which are specific to each type. The specificities of these mAbs were characterized previously (Sugiyama et al., 1994). A polyclonal antibody (pAb) against an 11–amino acid peptide (αpep6) of the COOH terminus of mouse IP_3R1 was also used (Nakade et al., 1994). The mAb against IP_3R3 (IgG_{2a} clone 2) was raised against amino acids 22–230 of the human IP_3R3 (Transduction Laboratories, Lexington, KY). The secondary antibody was an FITC-conjugated, anti–mouse IgG pAb that was adsorbed against rat serum (Vector Laboratories, Burlingame, CA). Subclass-specific secondary antibodies (FITC-conjugated goat anti–mouse IgG_1 pAb and Texas red–conjugated goat anti–mouse IgG_{2a} pAb) were purchased from Southern Biotechnology Associates, Inc. (Birmingham, AL).

Immunofluorescence

After being anesthetized with Nembutal, 8-wk-old rats were perfused with PBS followed by 4% paraformaldehyde in PBS. SMGs were dissected and postfixed for 2 h at 4°C. Cryosections (8 μm) were permeabilized with 0.05% Triton X-100 in PBS and treated with PBS containing 2% normal horse serum for 30 min at room temperature. The sections were then incubated with antibodies against IP_3R2 (2 μg/ml) and IP_3R3 (10 μg/ml). After washing, the sections were incubated with FITC-conjugated anti–mouse IgG. For double immunofluorescence staining of IP_3R2 and IP_3R3, we used Texas red–conjugated goat anti–mouse IgG_{2a} and FITC-conjugated goat anti–mouse IgG_1 secondary antibodies for KM1083 and KM1082, respectively. As a control, the antibody solutions were preadsorbed with a 10-fold excess of the peptide used to generate the primary mAb.

In Situ Hybridization

Frozen sections (12 μm) were prepared by cryostat sectioning, thaw-mounted onto gelatin-coated glass slides, and fixed for 15 min in 4% paraformaldehyde. By reverse transcriptase PCR, we generated two DNA probes, corresponding to the nucleotide position of 2920–4404 and 4609–5996 of the rat IP_3R2 cDNA sequence (Sudhof et al., 1991). Each fragment was cloned into the PCRII vector (Invitrogen Corp., Carlsbad, CA). Antisense and sense RNA probes were prepared by standard procedure using these two plasmid DNAs as templates. In situ hybridization was performed essentially as described by Furuichi and colleagues (1993).

Membrane Preparation and Western Blotting

SMGs of 8-wk-old male rats were removed and homogenized in a buffer containing 0.25 M sucrose, 1 mM EDTA, 0.1 mM PMSF, 10 μM leupeptin, 10 μM pepstatin A, 1 mM 2-mercaptoethanol, and 50 mM Tris-HCl, pH 7.4. The homogenates were centrifuged at 1,000 *g* for 5 min at 4°C. The supernatants were centrifuged at 105,000 *g* for 60 min at 2°C to sediment the membrane proteins. The pellets were resuspended in 8 M urea, 1 mM EDTA, 0.1 mM PMSF, 10 μM leupeptin, 10 μM pepstatin A, 1 μM 2-mercaptoethanol, and 50 mM Tris-HCl, pH 7.4. The membrane fractions dissolved in the sample buffer (4% sodium dodecyl sulfate, 12% glycerol [wt/vol], 50 mM Tris, 2% 2-mercaptoethanol [vol/vol], 0.01% Serva blue G, pH 6.8) were subjected to 5% Tricine–SDS-PAGE (Schagger and Jagow, 1987) containing 6 M urea, followed by electroblotting onto nitrocellulose membranes. The membranes were blocked with 5% skim milk and incubated with 40 ng/ml of each of the IP_3R mAbs. The bound mAbs were detected with the ECL system (Amersham Corp., Arlington Heights, IL). As a control, the antibody solutions were preadsorbed with a 10-fold excess of the peptide used to generate the primary mAb.

Electron Microscopy

We have developed a new technique that improves on previous preembedding techniques and has resulted in better images with good preservation (Katsumata et al., 1996). Briefly, the cryosections on glass slides were incubated first in a blocking solution, then with primary antibody, KM1083, overnight, and finally with anti–mouse IgG antibody conjugated with 0.8-nm gold colloids. The sections were rinsed with three changes of PBS at each step. The sections were postfixed with 2.5% glutaraldehyde, 0.2% tannic acid, and 1% OsO_4 in 0.1 M phosphate buffer for 30 min at room temperature, followed by a triple-distilled water rinse. Next, they were soaked in a solution for silver enhancement followed by three changes of distilled water. They were then embedded in a 1% chitoisan solution, dehydrated, and then processed routinely. Finally, the thin sections were stained with uranyl acetate and lead citrate and examined with an electron microscope (model JEX-1200EX; JEOL Ltd., Tokyo, Japan).

Ca^{2+} Imaging with a Real-Time Confocal Microscope

Wistar rats (8 wk old) were killed under deep anesthesia. The SMGs were excised immediately, trimmed of the capsule connective tissue, and cut into small pieces. They were digested with collagenase (2 mg/ml) in Eagle's minimal essential medium containing 25 mM Hepes, pH 7.4, for 45 min at 37°C with constant shaking and gentle pipetting (Segawa et al., 1985). The dissociated SMGs were then resuspended in a physiological salt solution (PSS) containing 135 mM NaCl, 5.8 mM KCl, 1.8 mM $CaCl_2$, 0.8 mM $MgSO_4$, 0.73 mM NaH_2PO_4, 11 mM glucose, 20 mM Hepes, pH 7.4, and 2 mM glutamine. The resuspended cells were incubated in the dark at 37°C for 30 min in the presence of 5 μM Indo-1-AM (Molecular Probes, Eugene, OR) or 10 μM Fluo-3-AM (Molecular Probes). After washing with PSS, they were mounted onto poly-L-lysine–coated cover glasses by Cytospin (Shandon, Cheshire, UK) centrifugation at 200 rpm and placed in a thermostatically controlled chamber at 37°C. Fluorescence was detected with a confocal laser scanning microscope (model RCM8000; Nikon Corp., Tokyo, Japan) with a 40× water immersion objective. Ducts and acini on the chamber were stimulated by perfusion with carbachol,

dissolved in PSS. Ca^{2+}-free solution was prepared by replacing 1.8 mM $CaCl_2$ by 1 mM EGTA.

Results

Polarized and Heterogeneous Distribution of IP_3R2 in the Duct Cells of Rat SMG

We investigated the localization of three distinct types of IP_3Rs throughout rat tissues with type-specific mAbs. Immunofluorescence using anti-IP_3R2 mAb (KM1083) showed that IP_3R2 was localized predominantly over the ducts in the rat SMG (Fig. 1 *A*). These ducts are composed of columnar cells lining the lumen. All staining was completely blocked by preincubation of the antibody with the antigen peptide (Fig. 1 *B*). At a higher magnification (Fig. 1 *C*), the strong immunosignals were concentrated in the apical cytoplasm. However, diffuse staining was also detected throughout the cytoplasm in the ductal cells. Heterogeneity was noted in the intensity of immunostaining among the duct cells. Extraordinarily strong immunostaining was found in certain ductal cells that were scattered throughout the granulated, striated, and exocretory ducts in intralobules. It was most remarkable in interlobular ducts (Figs. 1 *A* and 2 *A*). Weaker immunostaining with KM1083 was observed as well in apico-lateral regions of the acinar cells, corresponding to the intercellular canaliculi, the specialized lumen structure in the acini of rat SMG (Fig. 1, *A* and *C*).

Our in situ hybridization study confirmed that IP_3R2 expression in the SMG ducts was highest among all the tissues we analyzed. Silver grains representing the expression of IP_3R2 mRNA were concentrated in cells of the duct system (Fig. 1 *D*). The other components of the gland, including the secretory acini and the connective tissues, showed labeling at a level comparable to those on the control sections hybridized with a sense (control) probe (data not shown).

Colocalization of IP_3R2 and IP_3R3

The localization of two other IP_3R types, IP_3R1 and IP_3R3, in the rat SMG duct were also analyzed. The Abs against IP_3R1, KM1112 mAb and αpep6 pAb, did not give significant immunostaining in the duct system. We used two mAbs for detection of IP_3R3: KM1082 and IgG_{2a} clone 2, which recognized different sequences of IP_3R3 (see the Materials and Methods). Both anti-IP_3R3 mAbs gave weak and scattered immunosignals in apical regions of interlobular ductal epithelium and apico-lateral regions of the acinar cells (data not shown). Double immunostaining with KM1083 and KM1082 in the same section was also performed. Fig. 2, *A* and *B*, shows double-stained interlobular ducts (*arrows*), indicating that IP_3R3 coexists with IP_3R2 in the apical region. IP_3R3 was not detected in intralobular ducts (*arrowheads*). Because the immunosignal of KM1082 was relatively weak, a high concentration of KM1082 and a long photographic exposure were required to clearly localize IP_3R3, resulting in relatively high background. Staining from KM1082 outside of the apical region of the duct was also obtained in control sections (data not shown), so it was most likely nonspecific staining.

We also analyzed the expression of IP_3Rs in rat SMG by Western blotting using mAbs KM1112 for IP_3R1, KM1083 for IP_3R2, and KM1082 for IP_3R3. A band of ~240 kD was detected using each mAb (Fig. 3). As shown previously (Monkawa et al., 1995), the lower molecular–mass bands in the lanes of three IP_3Rs are proteolytic fragments of IP_3Rs. In our hands, these bands increased in intensity, and the bands of IP_3Rs were decreased by incubating the samples at 37°C for 6 h, suggesting proteolysis (data not shown). The 240-kD bands were abolished by preadsorption of the antibody with the antigen peptide, indicating that these antibodies specifically recognize each type of IP_3R protein expressed in the rat SMG.

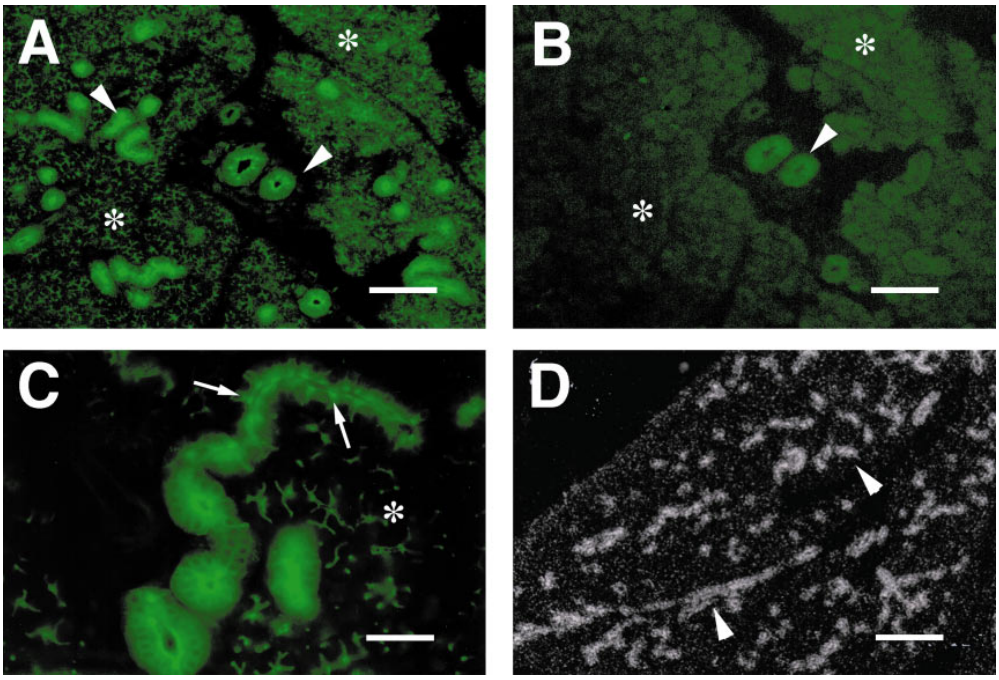

Figure 1. Localization of the IP_3R2 protein and mRNA in rat SMG. Immunohistochemical localization using mAb KM1083 (FITC-conjugated secondary) in low (*A*) and high (*C*) power views. (*B*) Preadsorption experiment using the immunizing antigen peptide, a control for *A*. Immunosignal was observed throughout the entire duct system, beneath luminal and lateral plasma membrane and in acinar cells. Arrowheads and asterisks indicate duct and acinus, respectively. The apical regions of cells with strong immunostaining are indicated by arrows in *C*. (*D*) In situ hybridization with antisense cRNA probes specific to IP_3R2. Arrowheads indicate duct. Bars: (*A* and *B*) 100 μm; (*C*) 25 μm; (*D*) 200 μm.

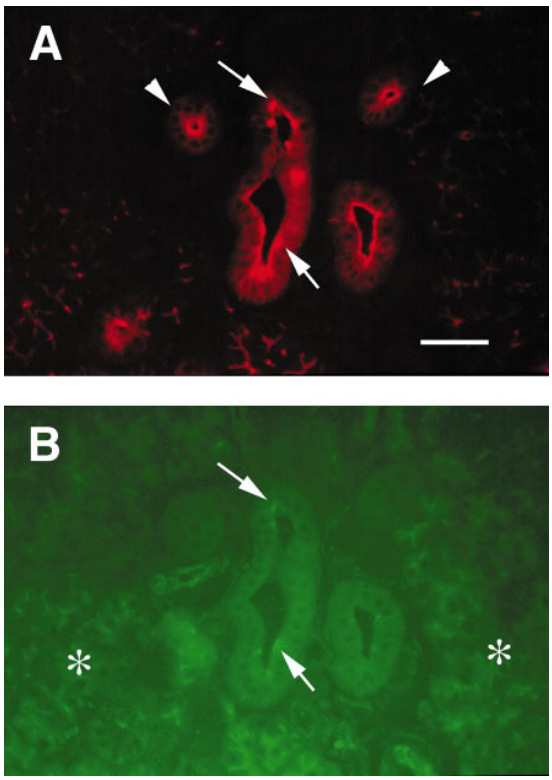

Figure 2. Colocalization of IP_3R2 and 3 in SMG ducts. (*A*) In the SMG, KM1083 immunoreactivity (Texas red–conjugated secondary) was observed in the apical pole of intralobular (*arrowheads*) and interlobular (*arrows*) duct cells. (*B*) KM1082 immunoreactivity (FITC-conjugated secondary) was also seen in the KM1083-positive region of interlobular duct (*arrows*). In the intralobular duct, immunosignal with KM1082 was observed, but it was below the detection capabilities of the imaging system. Asterisks indicate acinus. Bar, 25 μm.

Apical Small Vesicles Positive for IP_3R2

The ultrastructural localization of IP_3R2 in the duct cells was then examined by immunoelectron microscopy using the modified, preembedding silver enhancement method. As shown in Fig. 4, the silver grains were distributed mostly around small vesicles located in the apical cytoplasm of certain, but not all, duct cells. In this micrograph, relatively thin cytoplasm and short microvilli identified this as a "dark" cell (Sato and Miyoshi, 1988). Some principal cells in the striated and excretory ducts also possessed apical vesicles positive for IP_3R2. In the apical vesicles, silver grains were found mostly on the cytoplasmic side of the vesicle membrane, consistent with the fact that the epitope of the antibody is predicted to be on the cytoplasmic face. Other organelles, such as the rough ER, nuclei, and mitochondria, were mostly devoid of grains. No labeling was detected on the plasma membrane. These results suggested that among the duct cells, there was a specific population of cells that possess these apical vesicles bearing IP_3R2.

Carbachol-induced Ca^{2+} Wave Arose from the Apical Pole

Next we investigated the spatial and temporal distribution

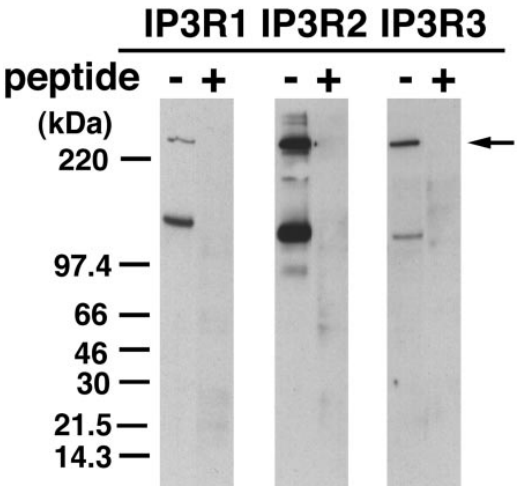

Figure 3. Immunoblot analysis of IP_3Rs in SMG. About 30 μg of membrane proteins were electrophoresed, transblotted, and probed with KM1112 (to IP_3R1), KM1083 (to IP_3R2), and KM1082 (to IP_3R3). "+" indicates control lanes in which each primary antibody was preadsorbed with the antigenic peptide before using it to probe the membrane. Arrow indicates the position of the IP_3Rs.

of Ca^{2+} in the ducts during stimulation by the phosphoinositide-coupled agonist, carbachol. We treated the rat SMG with collagenase to obtain dispersed pieces of ducts, which were then loaded with a Ca^{2+} indicator Indo-1. The lumen of the dissociated ducts was visualized by confocal imaging (Fig. 5 *A*). In the presence of extracellular Ca^{2+}, the ducts were continuously exposed to 10 μM carbachol. Fig. 5 *A* (a typical result of 20 such experiments) illustrates the spatial development of the cytoplasmic Ca^{2+} signal within the ducts. At rest (time = 0; Fig. 5 *A*, *a*), $[Ca^{2+}]_i$ was relatively low, although some localized moderate increases in $[Ca^{2+}]_i$ were detected in the basolateral periphery. The first increase of $[Ca^{2+}]_i$ was observed in the cytoplasm close to the apical plasma membrane of the cell (indicated

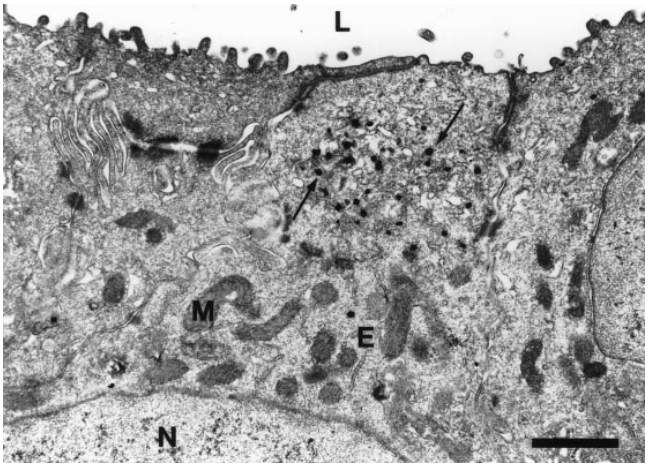

Figure 4. Ultrastructural localization of IP_3R2 in SMG duct cells using the modified preembedding silver-enhancement method. Immunosilver grains were observed on small vesicles beneath the plasma membrane (*arrows*). *E*, endoplasmic reticulum; *L*, lumen; *M*, mitochondria; *N*, nucleus. Bar, 0.1 μm.

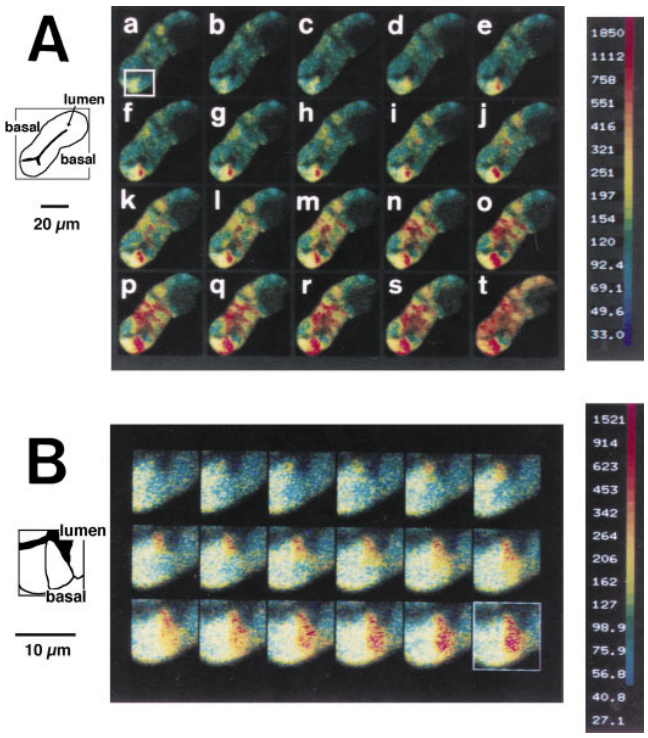

Figure 5. The spatial nature of the development of the cytoplasmic Ca^{2+} signal in an isolated duct. The two emission wavelengths of Indo-1 were acquired separately at video rate, stored at 15 ratio pairs/s, and then displayed in pseudocolor. The color scale was calibrated with the Calcium Calibration Buffer Kit II (Molecular Probes). (*A*, *a*) Application of 10 μM carbachol ($t = 0$). (*b–s*) A series of images at 330-ms intervals. *t*, an image 1 min after the beginning of the carbachol stimulation. (*B*) Images at 67-ms intervals showing the propagation of a Ca^{2+} wave at greater magnification within the cell enclosed in the square in Fig. 5 *A*, *a*.

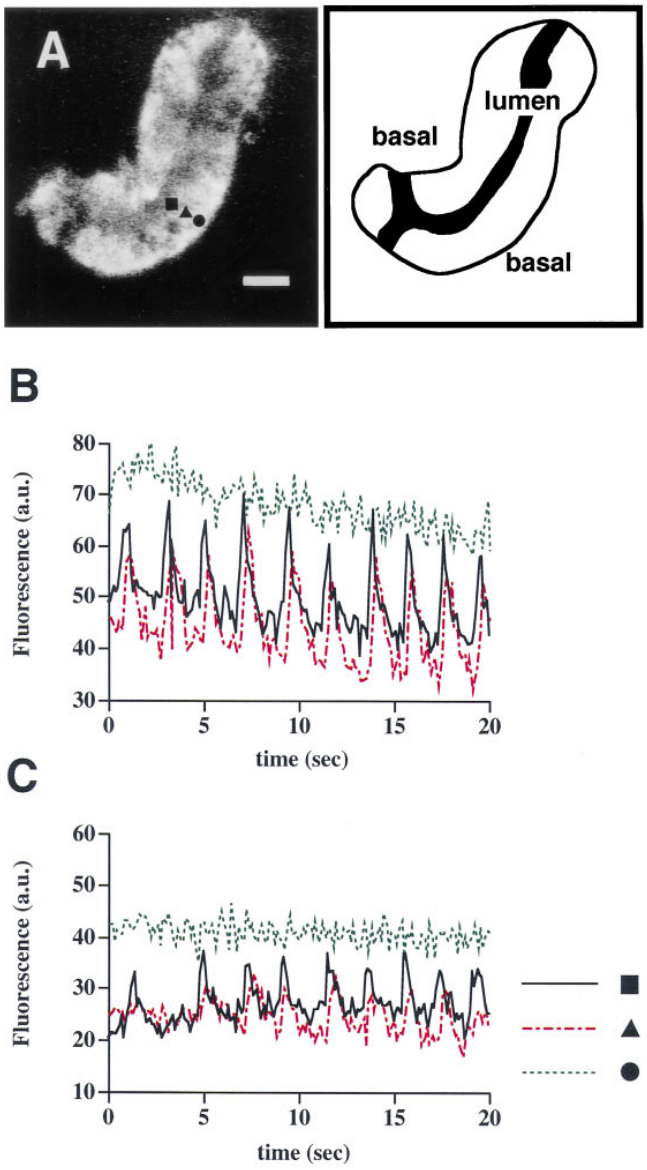

Figure 6. $[Ca^{2+}]_i$ oscillations observed in isolated ducts of rat SMG loaded with Fluo-3. Single-wavelength images were acquired at 30 Hz. (*A*) A snapshot of a duct 5 s after the beginning of the carbachol stimulation. (*B* and *C*) Time courses of fluorescence intensity from the three points across the cytoplasm of the cell shown in *A*. Apical (*square*), middle (*triangle*), basolateral (*circle*), when extracellular Ca^{2+} was present or absent, respectively. The $[Ca^{2+}]_i$ fluctuated at a frequency of around 0.5 Hz. Bar, 10 μm.

by an open square in Fig. 5 *A*, *a*) with a time lag of 1 s after stimulation (Fig. 5 *A*, *c*). This rise in $[Ca^{2+}]_i$ then spread, in a gradient fashion, toward the basolateral area. Fig. 5 *B* shows a series of digital images (every 67 ms) showing the progression of the carbachol-evoked $[Ca^{2+}]_i$ waves in the cell. Within about 1 s after the initial apical rise in $[Ca^{2+}]_i$, a complete elevation of $[Ca^{2+}]_i$ throughout the whole cytoplasm was observed. The front of the $[Ca^{2+}]_i$ transients moved at about 20 μm/s.

3–4 s after the beginning of the carbachol stimulation (Fig. 5 *A*, *h–k*), Ca^{2+} transients occurred also in the apical area of certain other cells. The $[Ca^{2+}]_i$ signals propagated toward the basolateral portions with a pattern similar to that seen in Fig. 5 *B*. When the carbachol-evoked calcium responses were fully developed (Fig. 5 *A*, *o–s*), $[Ca^{2+}]_i$ levels appeared to be homogeneous across the cytoplasm of these cells. But even at this stage, the $[Ca^{2+}]_i$ proved to change dynamically, as shown by the following detailed experiment.

Ca^{2+} Oscillations Observed by Video-Rate Confocal Microscopy

In an attempt to analyze the rapid Ca^{2+} response with greater precision, we used the nonratiometric Ca^{2+} indicator, Fluo-3, and observed $[Ca^{2+}]_i$ by video-rate confocal microscopy. We were able to see in greater detail $[Ca^{2+}]_i$ fluctuations induced by 10 μM carbachol in the presence of extracellular Ca^{2+}. Fig. 6 *B* gives a representative $[Ca^{2+}]_i$ transient observed in a cell; the time courses of $[Ca^{2+}]_i$ measured at three points across the cytoplasm of the cell (Fig. 6 *A*) are shown. In the apical Ca^{2+} initiation site, a short-lasting Ca^{2+} spike occurred, rapidly peaking at 250 ms, and decaying over 400–600 ms, with a frequency of around 0.5 Hz. Subsequently, the oscillatory $[Ca^{2+}]_i$ rises moved toward the basolateral area. The peaks of the $[Ca^{2+}]_i$ transients at the apical point (*square*) preceded the peak at the middle point (*triangle*) by 0.19 ± 0.07 s.

The distance between the two points was 4.7 μm. Thus, the velocity of the $[Ca^{2+}]_i$ wave in the cell was calculated to be 26 ± 7 μm/s (n = 7), which is similar to that characterized in Fig. 5 *B*. In the basolateral periphery (*circle*), small and continuous $[Ca^{2+}]_i$ transients were observed but were not statistically different from background noise (fluorescence intensity before stimulation, 66.5 ± 1.6 arbitrary units; after stimulation, 77.2 ± 2.8 arbitrary units, n = 12). These results indicated that the Ca^{2+} wave was confined to the apical-middle region.

To determine if extracellular Ca^{2+} participated in the $[Ca^{2+}]_i$ transients, measurements were performed without extracellular Ca^{2+}. Fig. 6 *C* shows the time course of $[Ca^{2+}]_i$ at three points as indicated in Fig. 6 *A*. The Ca^{2+} wave moved from the apical to the basolateral region of the cell with the same velocity, duration, and frequency as seen with extracellular Ca^{2+}, but with decreased amplitude. Thus, extracellular Ca^{2+} is not likely to be important for triggering the Ca^{2+} waves and oscillations. In the absence of extracellular Ca^{2+}, the Ca^{2+} waves disappeared ~50 s after the beginning of stimulation. However, the waves continued during stimulation when Ca^{2+} was present (data not shown).

Colocalization of the Ca^{2+} Initiation Sites with the Immunosignals for IP_3R2

In response to carbachol, Ca^{2+} spikes and subsequent Ca^{2+} waves took place only in certain ductal epithelial cells. Cells that were highly responsive to carbachol and those that were not were positioned randomly along the lumen (Fig. 5 *A*, *o–s*). We observed very heterogeneous $[Ca^{2+}]_i$ transients in 20 independent ductal preparations. We carried out immunohistochemistry on the ducts that had been used for the Ca^{2+} imaging experiments using KM1083 and an anti–mouse IgG secondary antibody conjugated to FITC. Fig. 7 *A* shows a $[Ca^{2+}]_i$ transient induced by carbachol in the apical cytoplasm in a cell. Likewise, in this same cell, a strong immunopositive signal of KM1083 colocalized with the rise in apical $[Ca^{2+}]_i$ (Fig. 7 *B*). In five out of six cells from three experiments, the Ca^{2+} initiation site also possessed significant amounts of IP_3R2.

Discussion

We investigated the intracellular and intercellular localization of IP_3Rs and correlated this with the initiation site of Ca^{2+} transient induced by agonist stimulation in ductal cell of the rat SMG. The Ca^{2+} signaling initiated primarily in the apical region of "pioneer cells," which expressed relatively high levels of IP_3Rs and evoked rapid and wavelike $[Ca^{2+}]_i$ transients after carbachol stimulation.

Polarized and Heterogeneous Localization of IP_3Rs in SMG Ducts

We showed that the distributions of IP_3R2 and IP_3R3 were predominantly in the apical poles of rat SMG duct cells (Figs. 1 and 2). The abundance of IP_3R2 mRNA was also shown by in situ hybridization (Fig. 1); among all the tissues tested, the SMG ducts gave highest hybridization signals. IP_3R3 was immunolocalized using two mAbs recognizing different epitopes (Fig. 2 *B*). Recently, Lee et al. (1997*a*) reported the localization of IP_3Rs in rat SMG ducts; IP_3R1 and IP_3R2 were localized close to the luminal and lateral membranes, and IP_3R3 around the nuclear envelope. These results differed from ours in the localizations of IP_3R1 and IP_3R3: (*a*) We did not detect any significant positive signals for IP_3R1 in the duct cells by either immunofluorescence or in situ hybridization (data not shown). The anti-IP_3R1 mAb, KM1112, has been shown to properly cross-react with rat IP_3R1 in tracheal and bronchiolar epithelia (Sugiyama et al., 1996), even though the peptide sequence used as an antigen to produce KM1112 was based on the human IP_3R1. Also, the 11 COOH-terminal amino acid sequence is common between rat and human IP_3R1s (Mignery et al., 1990; Yamada et al., 1994). So the fact that we did not detect IP_3R1 using KM1112 was not likely due to insufficient affinity of KM1112 to IP_3R1 in rat tissue. (*b*) In our study, IP_3R3 was not localized to the nuclear envelope but was colocalized with IP_3R2 on the apical side of the cell.

Previous electron microscopic studies showed that the ductal epithelium of rat SMG consists of several cell types, i.e., light, dark, tuft, and basal cells, most of which contain apical vesicles whose function remains unclear (Sato and Miyoshi, 1988). In the present study, using preembedding, silver-enhanced immunoelectron microscopy, we identified vesicular structures bearing IP_3R2 in the apical pole of some SMG duct cells (Fig. 4), which suggested that the apical vesicles might function as an intracellular Ca^{2+} pool. These vesicles were quite small (average size 20 nm in diameter) and did not appear similar to elements of the typical ER in Purkinje cell, which are IP_3-sensitive Ca^{2+} pools (Mignery et al., 1989). The characteristic shape of these apical vesicles resembles that of the "calciosome," which is believed to be an IP_3-regulated Ca^{2+} pool as differentiated portions of the ER in nonmuscle cells (Volpe et al., 1988; Pozzan et al., 1994). However, calciosomes were distributed throughout the cytoplasm in close apposition to the ER, which is quite different from the apical vesicles we have described in this study. It is interesting whether the apical vesicles we have described are also specialized ER components or something distinct from ER.

We found that only certain ductal cells expressed high levels of IP_3Rs in the apical region of the cell (Figs. 1 and 2). By three-dimensional, scanning confocal microscopy, we confirmed that the heterogeneity was clear at each level through the z-axis (data not shown). Our immunoelectron microscopy showed that certain "dark" and "principal" cells also had a large amount of IP_3R2 (Fig. 4; Segawa et al., 1996), so it is possible that any type of cell that expresses large amount of IP_3Rs may function as a pioneer cell (see below discussion).

Recently, upregulation of IP_3R expression during apoptosis has been reported (Khan et al., 1996), and it may be argued that the SMG duct cells exhibiting high IP_3R immunoreactivity are apoptotic. However, this seems unlikely since in our immunoelectron micrographs, we did not observe condensation of nuclear chromatin or any other apoptotic morphology (Kerr et al., 1972). Furthermore, we found hardly any DNA fragmentation in SMG duct cells (data not shown) by the TUNNEL method (Gavrieli et al., 1992).

The ryanodine receptor and ER Ca^{2+} pump are also ex-

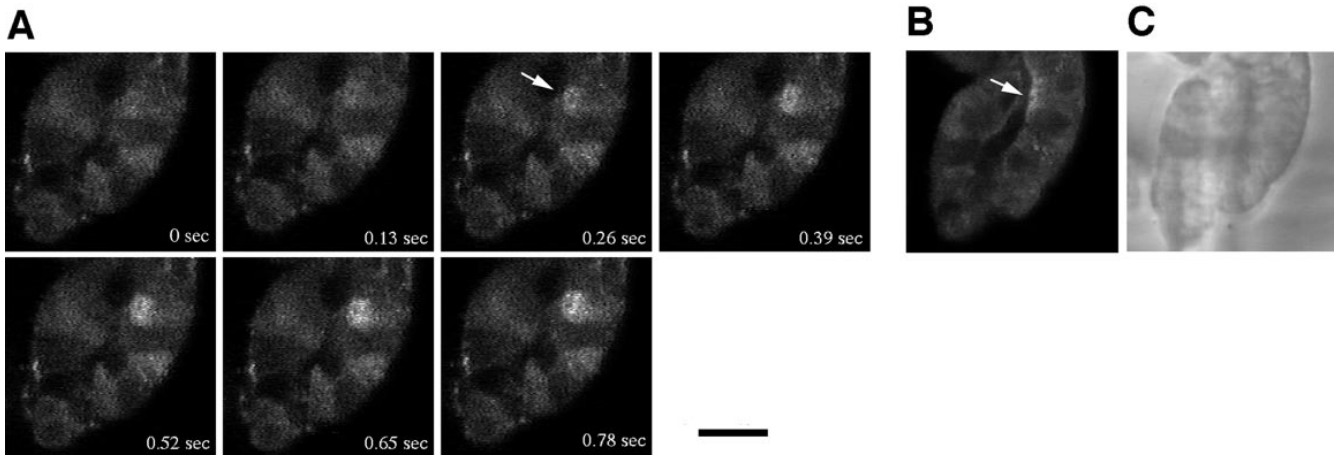

Figure 7. Colocalization of the $[Ca^{2+}]_i$ wave initiation site and IP_3R2-positive region. (*A*) Confocal images of the fluorescence intensity change of Fluo-3 in the duct cells. Times after stimulation (10^{-5} M carbachol) are indicated on each panel. (*B*) Confocal image of the immunofluorescence staining using KM1083 in the same duct shown in *A*. Arrows in *A* and *B* indicate the first $[Ca^{2+}]_i$ rise within the apical cytoplasm and immunosignal of IP_3R2, respectively. (*C*) Transmitted-light image. Bar, 10 μm.

pressed in the luminal pole of the SMG duct (Lee et al., 1997*a*,*b*). It would be interesting to know whether these molecules are also expressed heterogeneously among the ductal epithelial cells.

Intracellular Ca^{2+} Dynamics in SMG Ducts Relative to the Subcellular Localization of the IP_3Rs

Using real-time, confocal microscopy, we succeeded in visualizing $[Ca^{2+}]_i$ changes with high temporal and spatial resolution. The changes of $[Ca^{2+}]_i$ caused by carbachol were very rapid and dynamic. Our Ca^{2+} imaging demonstrated that Ca^{2+} spikes, local waves, and oscillations originated in the apical region of the duct cells (Figs. 5 and 6). Spatially restricted repetitive Ca^{2+} spikes described as "puffs" were also reported in mouse pancreatic acinar cells (Thorn et al., 1996) and in *Xenopus* oocytes (Yao et al., 1995; Berridge, 1997). When one compares Ca^{2+} spikes in rat SMG ducts with those in acinar cells and oocytes, the short-lasting Ca^{2+} spike in the SMG duct resembles the Ca^{2+} puffs in oocytes with respect to their short duration. However, the frequency of oscillations in SMG ducts was much faster than that in acinar cells or oocytes. Ca^{2+} puffs and spikes in pancreatic acinar cells are thought to be due to the opening of small clusters of IP_3Rs, but the relationship between the initiation site of Ca^{2+} spikes and the distribution of IP_3Rs has not been studied intensively in these cells. Here, we demonstrated the high-level expression of IP_3R2 and IP_3R3 at the Ca^{2+} wave initiation site (Fig. 7). Recently, Lee et al. (1997*a*) showed a correlation between the pattern of IP_3R expression and the initiation sites of Ca^{2+} waves in pancreatic and submandibular acinar cells. Our results, together with the data from Lee et al. (1997*a*), suggest that the apical concentration of IP_3Rs might be a general phenomenon in many other polarized epithelial cells.

While IP_3 signals are generated from the basolateral plasma membrane, the IP_3-induced increase in $[Ca^{2+}]_i$ occurs at the apical pole in these polarized cells, and unfortunately, the functional significance of the differential subcellular localizations of these two second messengers (between which cross talk is known to occur) is still unclear. Also, it is noteworthy that there is a considerable difference in the distance that Ca^{2+} and IP_3 can diffuse. In *Xenopus* oocytes, the diffusion lengths of IP_3, buffered Ca^{2+}, and free Ca^{2+} were measured to be 17, 3.6, and 0.08 μm, respectively (Allbritton et al., 1992). In pancreatic acinar cells, IP_3 was shown to act as a long-range messenger (Kasai and Petersen, 1994). In the case of SMG duct cells, therefore, IP_3Rs highly concentrated in the apical Ca^{2+} pools would be activated by IP_3 traveling from the basolateral region and would contribute to a polarized or gradient Ca^{2+} signal generated in the apical region, which might be prerequisite for efficient ductal functions.

Discrete Ca^{2+} Responses among Ductal Cells

In the present study, we demonstrated that the duct cells of the rat SMG did not respond to carbachol uniformly (Fig. 5). Pioneer cells showed rapid and dynamic $[Ca^{2+}]_i$ changes, while the less-reactive cells showed a slow and diffuse $[Ca^{2+}]_i$ transient. Other factors that might have produced such Ca^{2+} responses were considered, e.g., damage of cells caused by collagenase digestion or heterogeneous distribution of agonist receptor. However, in light of the fact that the distribution of the IP_3Rs completely overlapped with the Ca^{2+} initiation site (Fig. 7), we believe these to be unlikely explanations. The population of the cells highly expressing IP_3Rs in the duct was virtually identical to that of the cells highly reactive to carbachol. These observations indicated that the differential expression level of IP_3Rs was deeply correlated to the discrete Ca^{2+} response in individual duct cells.

The remaining problem is the characterization of the pioneer cell. The SMG duct consists of several cell types, so one of those previously identified may be functioning as the pioneer cell. Also, we have not shown conclusively that the pioneer cells controlled the change in $[Ca^{2+}]_i$ in the less-reactive cells in the manner of classical "pace maker" cells. However, our Ca^{2+} imaging suggested that

the Ca^{2+} wave that originated in the pioneer cells spread to the less-reactive cells. It should be easy to determine whether second messengers are diffusing from the pioneer cells to neighboring less-reactive cells or whether the spreading Ca^{2+} wave is independent of the pioneer cells.

The authors are grateful to Mr. O. Katsumata for technical assistance of the immunoelectron microscopy, the staff in Nikon Instech for the real time confocal microscopy, and Dr. David Zacharias for critical reading.

Received for publication 15 September 1997 and in revised form 9 February 1998.

References

Allbritton, N.L., T. Meyer, and L. Stryer. 1992. Range of messenger action of calcium ion and inositol 1,4,5-trisphosphate. *Science*. 258:1812–1815.

Berridge, M.J. 1993. Inositol trisphosphate and calcium signaling. *Nature*. 361: 315–325.

Berridge, M.J. 1997. Elementary and global aspects of calcium signalling. *J. Physiol. (Lond.)*. 499:290–306.

Dehaye, J.P., and R.J. Turner. 1991. Isolation and characterization of rat submandibular intralobular ducts. *Am. J. Physiol.* 261:c490–496.

Dehaye, J.P., I.H. Valdez, and R.J. Turner. 1993. Beta-adrenergic stimulation and cAMP mobilize Ca^{2+} from an IP_3-insensitive pool in rat submandibular granular ducts. *Am. J. Physiol.* 265:c1356–1362.

Furuichi, T., C.D. Simon, I. Fujino, N. Yamada, M. Hasegawa, A. Miyawaki, S. Yoshikawa, J. L. Guenet, and K. Mikoshiba. 1993. Widespread expression of inositol 1,4,5-trisphosphate receptor type 1 gene (Insp3r1) in the mouse central nervous system. *Recept. Channels*. 1:11–24.

Furuichi, T., K. Kohda, A. Miyawaki, and K. Mikoshiba. 1994. Intracellular channels [published erratum appears on 4(5):758]. *Curr. Opin. Neurobiol.* 4:294–303.

Gavrieli, Y., Y. Sherman, and S.S. Ben. 1992. Identification of programmed cell death in situ via specific labeling of nuclear DNA fragmentation. *J Cell Biol*. 119:493–501.

Khan, A.A., M.J. Soloski, A.H. Sharp, G. Schilling, D.M. Sabatini, S.H. Li, C.A. Ross, and S.H. Snyder. 1996. Lymphocyte apoptosis: mediation by increased type 3 inositol 1,4,5-trisphosphate receptor. *Science*. 273:503–507.

Kasai, H., and G.J. Augustine. 1990. Cytosolic Ca^{2+} gradients triggering unidirectional fluid secretion from exocrine pancreas. *Nature*. 348:735–738.

Kasai, H., and O.H. Petersen. 1994. Spatial dynamics of second messengers: IP_3 and cAMP as long-range and associative messengers. *Trends Neurosci.* 17: 95–101.

Kasai, H., Y.X. Li, and Y. Miyashita. 1993. Subcellular distribution of Ca^{2+} release channels underlying Ca^{2+} waves and oscillations in exocrine pancreas. *Cell*. 74:669–677.

Katsumata, O., E. Adachi, A. Segawa, S. Yamashina, C. Tadokoro, S.-Y. Song, and S. Kondo. 1996. An improved immuno-electron microscopy with a use of tannic acid and chitosan infiltration. *J. Electron Microsc*. 45:327.

Kerr, J.F., A.H. Wyllie, and A.R. Currie. 1972. Apoptosis: a basic biological phenomenon with wide-ranging implications in tissue kinetics. *Br. J. Cancer*. 26:239–257.

Lee, M.G., X, Xu, W. Zeng, J. Diaz, R.J.H. Wojcikiewicz, T.H. Kuo, F. Wuytack, L. Racymaekers, and S. Muallem. 1997*a*. Polarized expression of Ca^{2+} channels in pancreatic and salivary gland cells. *J. Biol. Chem*. 272: 15765–15770.

Lee, M.G., X, Xu, W. Zeng, J. Diaz, T.H. Kuo, F. Wuytack, L. Racymaekers, and S. Muallem. 1997*b*. Polarized expression of Ca^{2+} pumps in pancreatic and salivary gland cells. *J. Biol. Chem*. 272:15771–15776.

Maeda, N., T. Kawasaki, S. Nakade, N. Yokota, T. Taguchi, M. Kasai, and K. Mikoshiba. 1991. Structural and functional characterization of inositol 1,4,5-trisphosphate receptor channel from mouse cerebellum. *J. Biol. Chem*. 266: 1109–1116.

Mignery, G.A., T.C. Sudhof, K. Takei, and C.P. De. 1989. Putative receptor for inositol 1,4,5-trisphosphate similar to ryanodine receptor. *Nature*. 342:192–195.

Mignery, G.A., C.L. Newton, B.T. Archer, and T.C. Sudhof. 1990. Structure and expression of the rat inositol 1,4,5-trisphosphate receptor. *J. Biol. Chem*. 265:12679–12685.

Monkawa, T., A. Miyawaki, T. Sugiyama, H. Yoneshima, H.M. Yamamoto, T. Furuichi, T. Saruta, M. Hasegawa, and K. Mikoshiba. 1995. Heterotetrameric complex formation of inositol 1,4,5-trisphosphate receptor subunits. *J. Biol. Chem*. 270:14700–14704.

Nakade, S., S.K. Rhee, H. Hamanaka, and K. Mikoshiba. 1994. Cyclic AMP-dependent phosphorylation of an immunoaffinity-purified homotetrameric inositol 1,4,5-trisphosphate receptor (type I) increases Ca^{2+} flux in reconstituted lipid vesicles. *J. Biol. Chem*. 269:6735–6742.

Nathanson, M.H., A.D. Burgstahler, and M.B. Fallon. 1994. Multistep mechanism of polarized Ca^{2+} wave patterns in hepatocytes. *Am. J. Physiol.* 267: g338–349.

Pozzan, T., R. Rizzut, P. Volpe, and J. Meldolesi. 1994. Molecular and cellular physiology of intracellular calcium stores. *Physiol. Rev*. 74:595–636.

Sato, A., and S. Miyoshi. 1988. Ultrastructure of the main excretory duct epithelia of the rat parotid and submandibular glands with a review of the literature. *Anat. Rec.* 220:239–251.

Schagger, H., and G.V. Jagow. 1987. Tricine-sodium dodecyl sulfate-PAGE for the separation of proteins in the range from 1 to 100 kD. *Anal. Biochem.* 166:368–379.

Segawa, A., N. Sahara, K. Suzuki, and S. Yamashina. 1985. Acinar structure and membrane regionalization as a prerequisite for exocrine secretion in the rat submandibular gland. *J. Cell Sci.* 78:67–85.

Segawa, A., M. Hino, T. Sugiyama, M. Hasegawa, A. Miyawaki, T. Furuichi, K. Mikoshiba, E. Adachi, O. Katsumata, and S. Yamashina. 1996. Ultrastructural immunolocalization of IP_3 receptor in the rat submandibular gland duct cells. *J. Electron Microsc.* 45:327.

Sudhof, T.C., C.L. Newton, B.T. Archer III, Y.A. Ushkaryov, and G.A. Mignery. 1991. Structure of a novel InsP3 receptor. *EMBO (Eur. Mol. Biol. Organ.) J.* 10:3199–3206

Sugiyama, T., A. Furuya, T. Monkawa, H.M. Yamamoto, S. Satoh, K. Ohmori, A. Miyawaki, N. Hanai, K. Mikoshiba, and M. Hasegawa. 1994. Monoclonal antibodies distinctively recognizing the subtypes of inositol 1,4,5-trisphosphate receptor: application to the studies on inflammatory cells. *FEBS Lett.* 354:149–154.

Sugiyama, T., H.M. Yamamoto, K. Wasano, K. Mikoshiba, and M. Hasegawa. 1996. Subtype-specific expression patterns of inositol 1,4,5-trisphosphate receptors in rat airway epithelial cells. *J. Histochem. Cytochem*. 44:1237–1242.

Thorn, P., A.M. Lawrie, P.M. Smith, D.V. Gallacher, and O.H. Petersen. 1993. Local and global cytosolic Ca^{2+} oscillations in exocrine cells evoked by agonists and inositol trisphosphate. *Cell*. 74:661–668.

Thorn, P., R. Moreton, and M. Berridge. 1996. Multiple, coordinated Ca^{2+}-release events underlie the inositol trisphosphate-induced local Ca^{2+} spikes in mouse pancreatic acinar cells. *EMBO (Eur. Mol. Biol. Organ.) J.* 15:999–1003.

Valdez, I.H., and R.J. Turner. 1991. Effects of secretagogues on cytosolic Ca^{2+} levels in rat submandibular granular ducts and acini. *Am. J. Physiol.* 261: G359–G363.

Volpe, P., K.H. Krause, S. Hashimoto, F. Zorzato, T. Pozzan, J. Meldolesi, and D.P. Lew. 1988. "Calciosome," a cytoplasmic organelle: the inositol 1,4,5-trisphosphate-sensitive Ca^{2+} store of nonmuscle cells? *Proc. Natl. Acad. Sci. USA*. 85:1091–1095.

Xu, X., J. Diaz, H. Zhao, and S. Muallem. 1996. Characterization, localization and axial distribution of Ca^{2+} signaling receptors in the rat submandibular salivary gland ducts. *J. Physiol. (Lond.)*. 491:647–662.

Yamada, N., Y. Makino, R.A. Clark, D.W. Pearson, M.G. Mattei, J.L. Guenet, E. Ohama, I. Fujino, A. Miyawaki, T. Furuichi, and K. Mikoshiba. 1994. Human inositol 1,4,5-trisphosphate type 1 receptor, InsP3R1: structure, function, regulation of expression and chromosomal localization. *Biochem. J.* 302:781–790.

Yao, Y., J. Choi, and I. Parker. 1995. Quantal puffs of intracellular Ca^{2+} evoked by inositol trisphosphate in Xenopus oocytes. *J. Physiol. (Lond.)*. 482:533–553.